Computational Transonic Flutter Boundary Tracking Procedure

John W. Gallman*
Purdue University, West Lafayette, Indiana
John T. Batina†
NASA Langley Research Center, Hampton, Virginia
and
T.Y. Yang‡
Purdue University, West Lafayette, Indiana

An automated flutter boundary tracking procedure is presented for the efficient calculation of transonic flutter boundaries. The new procedure uses aeroelastic responses to march along the boundary by taking steps in speed and Mach number, thereby reducing the number of response calculations previously required to determine a transonic flutter boundary. The tracking procedure reduces computational costs because only two response calculations are required per Mach number and provides a complete boundary in a single job submission. Flutter boundary results are presented for a typical airfoil section oscillating with pitch and plunge degrees of freedom. These transonic flutter boundaries are in good agreement with "exact" boundaries calculated using the conventional time-marching method. The tracking procedure was also extended to include static aeroelastic twist as a simulation of the static deformation of a wing and thus contains all of the essential features required to apply it to practical three-dimensional cases. Application of the procedure is also made to flutter boundaries as a function of structural parameters, the capability of which is useful as a design tool.

Nomenclature

a = nondimensional elastic axis location, positive aft of midchord
b = airfoil semichord
c = airfoil chord
c_ℓ = lift coefficient
c_m = moment coefficient about pitching axis
h = plunge displacement, positive down
$[K]$ = structural stiffness matrix
K_α = pitch spring constant
m = airfoil mass per unit span
M = freestream Mach number
$[M]$ = structural mass matrix
r_α, r_{cg} = airfoil radii of gyration about elastic axis and center of gravity
s = Laplace transform variable, $\sigma + i\omega$
t = time, s
U, U_f = freestream velocity and flutter speed, respectively
V, V_f = speed index $U/(b\omega_\alpha\sqrt{\mu})$ and flutter speed index $U_f/(b\omega_\alpha\sqrt{\mu})$
x = distance aft of leading edge
x_α = nondimensional distance from elastic axis to mass center
α = airfoil angle of attack, positive leading edge up
α_0 = airfoil mean angle of attack
α_r = wing root angle of attack
ζ = dominant damping of aeroelastic response, positive for stable response
μ = airfoil mass ratio, $m/\pi\rho b^2$
ρ = freestream air density
σ = damping coefficient of Laplace transform variable
ω = frequency of aeroelastic response
ω_h, ω_α = uncoupled plunge and pitch natural frequencies, respectively

Received May 19, 1986; presented as Paper 86-0902 at the AIAA/ASME/ASCE/AHS 27th Structures, Structural Dynamics and Materials Conference, San Antonio, TX, May 19-21, 1986; revision received Jan. 20, 1987.

*Graduate Research Assistant, School of Aeronautics and Astronautics.
†Research Scientist, Unsteady Aerodynamics Branch, Loads and Aeroelasticity Division. Senior Member AIAA.
‡Professor and Dean, Schools of Engineering. Fellow AIAA.

Introduction

FLUTTER is frequently a limiting factor in the performance of aircraft in transonic flight. Because of this limitation, it is highly desirable to be able to predict transonic flutter characteristics accurately, especially during aircraft design. Furthermore, since design is an iterative process, it is important to be able to perform transonic flutter calculations inexpensively.

Research on developing nonlinear transonic flutter prediction techniques has progressed with the development of transonic small-disturbance (TSD) computer codes. The nonlinear techniques typically require the calculation of time responses to determine the stability of the aeroelastic system. In the time response analysis, the structural equations of motion are coupled to transonic aerodynamic codes using a numerical integration procedure. For example, Ballhaus and Goorjian[1] first reported the calculation of transonic aeroelastic responses for an oscillating airfoil with a single pitching degree of freedom (DOF). Time responses were presented for the NACA 64A006 airfoil at $M=0.88$. The calculations were performed by simultaneously integrating the structural equation of motion with the unsteady aerodynamic solution procedure of their LTRAN2 code.[2]

The time-marching aeroelastic solution technique has subsequently been refined and extended by a number of researchers. Guruswamy and Yang[3] performed aeroelastic response calculations for a plunging and pitching NACA 64A006 airfoil at $M=0.85$. Flutter speeds selected from a separate flutter analysis indeed resulted in neutrally stable time responses. Time-marching aeroelastic responses for airfoils including an aileron pitching DOF were presented in

Refs. 4-6. Rizzetta[4] demonstrated significant nonlinear effects using relatively large initial conditions. Yang and Chen[5] and Yang and Batina[6] presented three DOF time response results for the NACA 64A006, NACA 64A010, and MBB-A3 airfoils. Edwards et al.[7] presented nonlinear transonic flutter boundaries including angle-of-attack effects. The results were obtained using a more accurate structural integrator that was based on the state transition matrix. More recently, Batina and Yang[8] have investigated the effects of active controls on transonic aeroelastic responses and subsequently assessed the accuracy of state-space aeroelastic modeling. Berry et al.[9] have included viscous effects in the calculation of transonic aeroelastic responses by using an integral boundary-layer routine coupled to an inviscid TSD code. Furthermore, Borland and Rizzetta[10] have applied the time-marching aeroelastic response technique to a three-dimensional case. In Ref. 10, nonlinear transonic flutter results were reported for a rectangular wing with parabolic arc airfoil section.

Although the time-marching aeroelastic procedures are relatively well developed for the determination of transonic flutter boundaries, the method can require large amounts of computer resources. In general, several aeroelastic responses need to be calculated for a range of flight speeds at a given Mach number. The flutter point is then estimated by interpolation of the damping from stable and unstable responses. To determine the flutter boundary, the procedure is repeated for each Mach number of interest. The repetitive nature of the time-marching aeroelastic method (hereafter referred to as the conventional method) can be computationally quite expensive as well as manpower intensive. The calculation of a transonic flutter boundary, for example, can require as much as 2–4 weeks of elapsed analysis time.

What is needed is a second generation method, which is less expensive and time consuming. Therefore, it is the purpose of this paper to present the development of a transonic flutter boundary tracking procedure that significantly reduces the elapsed analysis time and lowers computational costs. The objectives of this research were: 1) to develop an efficient automated flutter boundary tracking procedure which utilizes a time-marching aeroelastic response code, 2) to verify the procedure by making detailed comparisons with conventional flutter solutions, 3) to improve the procedure by including static aeroelastic twist, and 4) to demonstrate the robustness and utility of the new procedure by applying it to a variety of aeroelastic cases.

In this study, the tracking procedure is applied to a simple aeroelastic system consisting of a typical airfoil section oscillating with pitch and plunge degrees of freedom. The procedure is coupled to the time-marching aeroelastic response analysis within the XTRAN2L[11] unsteady transonic small-disturbance code. Time-marching aeroelastic solutions and their application to the conventional method is described. A more detailed description is given of the flutter boundary tracking procedure including the step-by-step numerical implementation. The inclusion of static aeroelastic twist into the calculations to simulate static deformation under load is also described. Finally, representative results and comparisons assessing the tracking procedure are presented.

Time-Marching Aeroelastic Solutions

The equations of motion for a typical airfoil section with pitch and plunge degrees of freedom may be written in matrix form as[7]

$$[M]\begin{Bmatrix}\ddot{h}\\ \ddot{\alpha}\end{Bmatrix}+[K]\begin{Bmatrix}h\\ \alpha\end{Bmatrix}=\frac{1}{\pi\mu}\left(\frac{U}{b}\right)^2\begin{Bmatrix}-(c_\ell-c_{\ell_0})\\ 2(c_m-c_{m_0})\end{Bmatrix} \tag{1}$$

where $[M]$ is the mass matrix, $[K]$ is the stiffness matrix, and $(\dot{})$ denotes differentiation with respect to time t. Plunge and pitch displacements h and α, respectively, are perturbations about the mean airfoil position. The lift and moment coefficients c_{ℓ_0} and c_{m_0}, respectively, are the steady-state values calculated at the mean angle of attack α_0, which are subtracted from the total coefficients. In the time-marching solution, the equations of motion are coupled to an unsteady aerodynamic code for time integration. In this study, Eq. (1) is simultaneously integrated with the aerodynamic solution procedure of the XTRAN2L code using the modified state transition matrix integrator of Edwards et al.[7] Details of the solution procedure may be found in Ref. 7. An initial plunge displacement is typically used to start the integration of Eq. (1) by setting $h(0)=0.01$ and $\alpha(0)=\dot{h}(0)=\dot{\alpha}(0)=0$.

In the conventional method, the flutter analyst must repetitively calculate time-marching aeroelastic responses for a range of speeds U at a given Mach number. Generally, three or four speeds are selected for response calculations to determine one stable and one unstable flight speed. The flutter speed U_f is calculated by interpolating the dominant damping of the responses to the speed where damping is zero. The procedure is then repeated for each Mach number of interest.

Damping of the aeroelastic responses is estimated from the response curves using the modal identification technique of Bennett and Desmarais.[12] The modal estimates are determined by a least squares curve fit of the responses using complex exponential functions of the form

$$X(t)=A_0+\sum_{j=1}^{m}e^{\sigma_j t}[A_j\cos(\omega_j t)+B_j\sin(\omega_j t)] \tag{2}$$

where m is the number of modes selected here to be equal to two. The damping of each mode is calculated using

$$\zeta_j=-\sigma_j/\sqrt{\sigma_j^2+\omega_j^2} \tag{3}$$

The dominant damping of the aeroelastic system is determined by selecting the smallest value of ζ_j. As an example, the top part of Fig. 1 shows a typical pitch response and modal curve fit. In the lower part of Fig. 1 are the two component modes determined from the modal fit. As shown in Fig. 1, the lower-

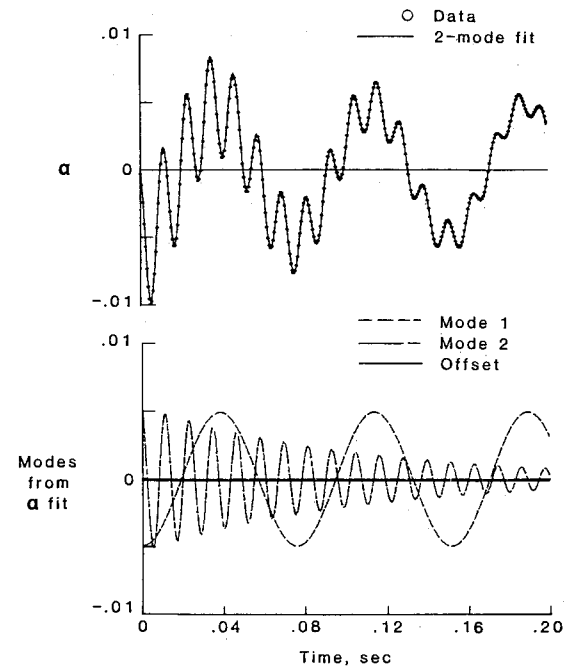

Fig. 1 Modal curve fit of aeroelastic pitch response and resulting component modes at flutter for the NACA 64A010A airfoil at $M=0.80$.

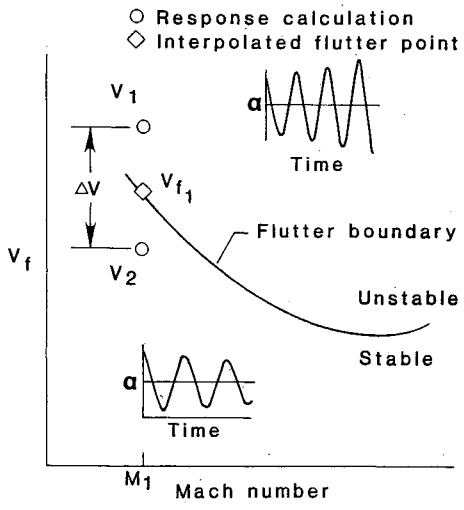

a) Calculation of first flutter speed index V_{f_1} and starting conditions

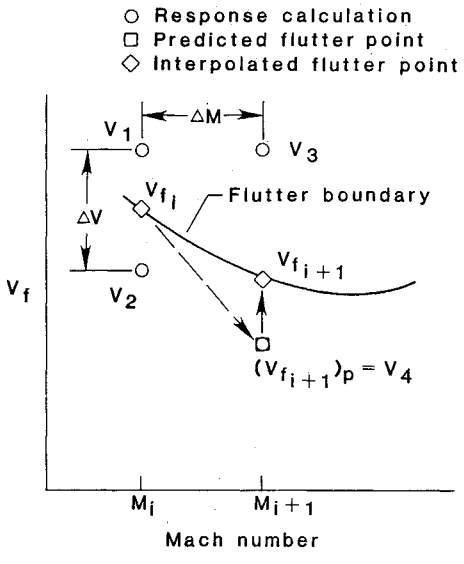

b) Flutter boundary tracking from Mach number M_i to M_{i+1}

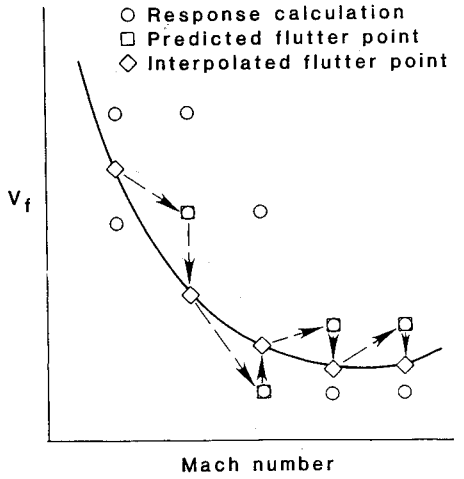

c) Continuation of tracking procedure over a range of Mach number values

Fig. 2 Graphical description of flutter boundary tracking procedure.

frequency, constant-amplitude mode is dominant and therefore determines the stability of the aeroelastic system.

In the conventional method, the modal identification code of Ref. 12 is normally run as a separate job step. Based upon the results of this program, the flutter analyst must then make decisions on continuing the solution procedure. Therefore, the method can be quite manpower intensive with the calculation of a transonic flutter boundary requiring as much as 2–4 weeks of elapsed analysis time.

Flutter Boundary Tracking Procedure

The flutter boundary tracking procedure is an algorithm for calculating a transonic flutter boundary in an efficient and automated fashion. In this study, the procedure is coupled to the time-marching aeroelastic response analysis within the XTRAN2L code. However, the procedure is general enough to be coupled to any aeroelastic response code.

Starting conditions are required to begin the flutter boundary tracking procedure at Mach number M_1, as shown in Fig. 2a. The starting conditions are obtained within the tracking procedure code using the conventional method. Several responses are computed for varying speed indices to determine values V_1 and V_2 that bracket the flutter boundary. The first flutter speed index V_{f_1} is calculated by interpolation of the dominant damping of these responses. The starting conditions for the tracking procedure at Mach number M_1 include the speed indices V_1 and V_2, the dominant damping values of the responses at these speeds ζ_1 and ζ_2, respectively, and the flutter speed index V_{f_1}.

The procedure tracks the boundary from a given Mach number M_i to M_{i+1} as shown in Fig. 2b. The flutter speed index V_{f_i} is assumed to be known. The flutter speed index at M_{i+1} is predicted by approximating the flutter boundary curve with the Taylor series,

$$V_{f_{i+1}} = V_{f_i} + \frac{dV}{dM}(M_{i+1} - M_i) + \frac{1}{2!}\frac{d^2V}{dM^2}(M_{i+1} - M_i)^2 + \ldots \quad (4)$$

Since relatively small steps in Mach number are used, all terms of second- or higher-order are neglected. Since $V = f(M)$ is an implicit function specified by $\zeta(V,M) = 0$, the slope of the flutter boundary can be expressed as $dV/dM = -(\partial\zeta/\partial M)/(\partial\zeta/\partial V)$. Rewriting Eq. (4) in delta notation gives

$$V_{f_{i+1}} = V_{f_i} - \frac{\Delta\zeta_M/\Delta M}{\Delta\zeta_V/\Delta V}(M_{i+1} - M_i) \quad (5)$$

The change in damping terms are defined as

$$\Delta\zeta_V = \zeta(V_1, M_i) - \zeta(V_2, M_i) \quad (6a)$$

$$\Delta\zeta_M = \zeta(V_3, M_{i+1}) - \zeta(V_1, M_i), \text{ if } V_3 = V_1 \quad (6b)$$

$$\Delta\zeta_M = \zeta(V_3, M_{i+1}) - \zeta(V_2, M_i), \text{ if } V_3 = V_2 \quad (6c)$$

and the terms ΔV and ΔM are expressed as

$$\Delta V = V_1 - V_2 \quad (7a)$$

$$\Delta M = M_{i+1} - M_i \quad (7b)$$

where ζ is the damping of the dominant mode of the aeroelastic response calculated for the given speed index and Mach number combination. The speed indices V_1, V_2, and V_3 are the values at which response calculations are performed. Equations (5–7) form the basis of the flutter boundary tracking procedure.

Computationally, the procedure tracks the boundary from Mach number M_i to M_{i+1} as follows:

1) A converged steady flowfield is calculated at conditions (V_{fi},M_i) to be used as the initial flowfield for aeroelastic response calculations at M_{i+1}. For the values of ΔM investigated, the numerical transient induced by using an initial flowfield at a neighboring Mach number is negligible.

2) To determine the flutter speed index at Mach number M_{i+1}, aeroelastic responses are calculated at the speed index V_3 shown in Fig. 2b. The dominant damping of these responses is then determined for the evaluation of the $\Delta\zeta_M/\Delta M$ term in Eq. (5). The $\Delta\zeta_V/\Delta V$ term in Eq. (5) is calculated from information already known at M_i. For the first prediction of V_{fi+1} from V_{fi} with Eq. (5), the value of the speed index V_3 is set equal to V_1. For all other predictions, the speed index V_3 is set equal to V_1 if the absolute value of $(V_{fi}-V_1)$ is less than the absolute value of $(V_{fi}-V_2)$. Otherwise, V_3 is set equal to V_2. The predicted flutter point determined using Eq. (5) is labeled $(V_{fi+1})p$ in Fig. 2b.

3) Aeroelastic response histories are calculated at V_4, which is set equal to $(V_{fi+1})p$ to determine the stability of the airfoil at the predicted flutter speed index. The dominant damping values obtained from the responses calculated at V_3 and V_4 are then used to calculate the final flutter speed index V_{fi+1} by interpolation or extrapolation of the damping. Figure 2b shows a typical interpolation case.

4) The procedure is continued to the next Mach number by returning to step 1 for the calculation of a new converged steady flowfield. When returning to step 1, the values for V_1, V_2, ζ_1, ζ_2, V_{fi}, and M_i are set equal to V_3, V_4, ζ_3, ζ_4, V_{fi+1}, and M_{i+1}, respectively. By repeating steps 1–4 for a range of Mach number values, a flutter boundary can be calculated as shown graphically in Fig. 2c.

Additionally, the flutter boundary tracking procedure is not constrained to determine flutter boundaries as a function of Mach number. The current implementation of the procedure allows for the calculation of flutter boundaries with respect to an aeroelastic parameter such as μ, a, x_α, r_α, ω_h, or ω_α instead of Mach number. In this case, the mathematical formulation of the tracking procedure is the same as that described above with the chosen parameter being substituted for Mach number M. Computationally, the parameter and the corresponding step are chosen as input.

Static Aeroelastic Twist

To be able to conceptually apply the tracking procedure to realistic three-dimensional cases, the procedure was extended to include static aeroelastic twist as a two-dimensional simulation of the static deformation of a wing. The significance of static aeroelastic twist on typical section flutter at transonic speeds was demonstrated by Edwards et al.[7] The static twist is determined by using a simple model of a linear root pitch spring and equating the aerodynamic pitching moment to the pitch spring restoring moment. The resulting static equilibrium equation may be written as

$$K_\alpha(\alpha_0-\alpha_r)=\tfrac{1}{2}\rho U^2(2b)^2c_{m_0}(\alpha_0,M) \tag{8}$$

where $(\alpha_0-\alpha_r)$ is the static aeroelastic twist. In terms of a strip theory analysis, α_r is the wing root angle of attack and α_0 is the local section mean angle of attack. The steady-state moment coefficient about the pitching axis c_{m_0} is the same quantity that appears in Eq. (1). By nondimensionalizing, Eq. (8) may be rewritten as

$$\alpha_0=\alpha_r+\frac{2V^2}{\pi r_\alpha^2}c_{m_0}(\alpha_0,M) \tag{9}$$

which is solved iteratively for the mean angle of attack α_0.

The mean angle of attack must be calculated to include static aeroelastic effects in flutter boundary calculations. By modifying XTRAN2L to include Eq. (9), a steady flowfield and mean angle of attack are obtained simultaneously. Specifically, the wing root angle of attack α_r is fixed and α_0 is varied until a converged steady flowfield and mean angle of attack α_0 are determined. For application to the conventional method, a static aeroelastic calculation should be performed before each response calculation. This adds the computational cost of performing one steady flowfield calculation per response to the total cost of a conventional method flutter solution. When including static aeroelastic twist in the flutter boundary tracking procedure, the mean angle of attack α_0 is determined during the steady flowfield calculation in step 1. For the cases presented a converged steady flowfield and mean angle of attack α_0 are obtained in the same number of time steps required for the steady flowfield calculation without static twist. Consequently, static twist is included in the tracking procedure at no additional cost. The mean angle of attack used for all response calculations at M_{i+1} is set equal to the mean angle of attack calculated for flutter at M_i. For the values of ΔV and ΔM investigated, the changes in mean angle of attack α_0 when stepping from M_i to M_{i+1} were small. Consequently, the static aeroelastic twist is lagged one Mach number for computational convenience.

Results and Discussion

Flutter boundary calculations were performed for a typical airfoil section oscillating with pitch and plunge degrees of freedom. The airfoils chosen were the NACA 64A010 NASA Ames model (herein referred to as NACA 64A010A) and the MBB-A3 supercritical airfoil. The airfoil coordinates were taken from Ref. 13. Flutter boundary results are presented for Case A of Isogai,[14,15] which has normal modes similar to those of a streamwise section near the tip of a swept-back wing. The wind-off coupled plunge and pitch frequencies are 71.33 and 535.65 rad/s, respectively. The pivotal point for the plunge mode is located 1.44 chord lengths ahead of the leading edge. The pivotal point for the pitch mode is 0.068 chord lengths forward of midchord. Specifically, the aeroelastic parameter values are $a=-2.0$, $x_\alpha=1.8$, $r_\alpha=1.865$, $\mu=60.0$, $\omega_h=100$ rad/s, and $\omega_\alpha=100$ rad/s.

Flutter Boundary Tracking Results

Calculations were performed for the NACA 64A010A and MBB-A3 airfoils for Mach numbers of $M=0.65$–0.80. The mean angles of attack were $\alpha_0=1.0$ deg for the NACA 64A010A airfoil and $\alpha_0=-0.5$ deg for the MBB-A3 airfoil. These angles of attack were chosen by Bland and Edwards[16] for these airfoils, because they produce steady-state lift and shock locations that are approximately equal at the same Mach number. With lift and shock locations approximately equal, comparisons of flutter behavior can be made between the two airfoils. Steady pressure distributions for the NACA 64A010A and MBB-A3 airfoils are shown in Figs. 3a and 3b, respectively, for Mach numbers of $M=0.75$–0.80 in increments of 0.01. For the NACA 64A010A airfoil (Fig. 3a), the flow is subcritical up to approximately $M=0.76$. Between $M=0.76$ and 0.77, a shock wave forms on the upper surface near 45% chord. With increasing Mach number, the shock grows in strength and moves further downstream along the airfoil. The shock becomes relatively strong and is located near 68% chord at $M=0.80$. For the MBB-A3 airfoil (Fig. 3b), the steady pressure distributions behave in much the same manner as for the NACA 64A010A airfoil. The upper surface shock wave forms between $M=0.77$ and 0.78 and grows in strength with increasing Mach number. At $M=0.80$, the shock is located at 68% chord, which is the same as that for the NACA 64A010A airfoil. The strength of the MBB-A3 shock wave, however, is considerably less. Furthermore, the pitching moment (about quarter chord) for the MBB-A3 airfoil is much different in comparison with the NACA 64A010A airfoil because of the aft loading.

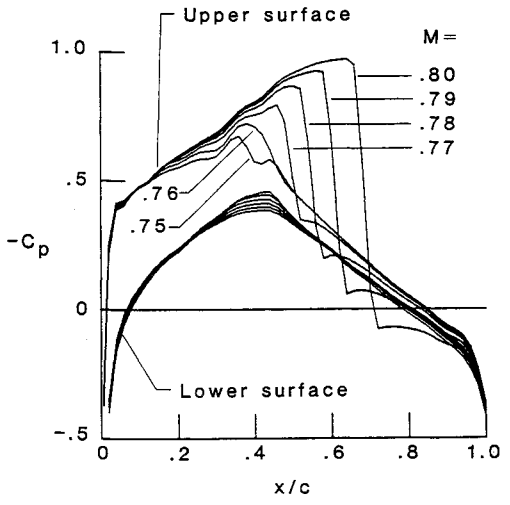

a) NACA 64A010A airfoil at $\alpha_0 = 1.0$ deg

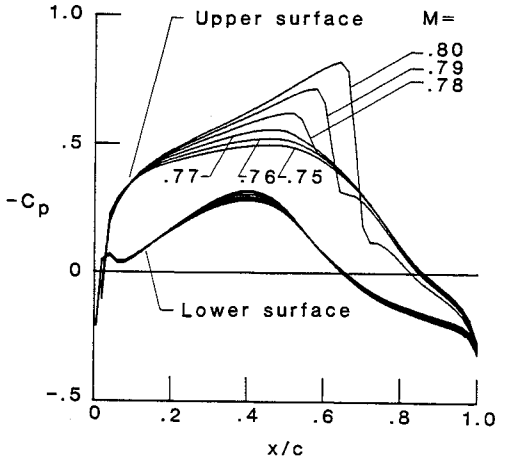

b) MBB-A3 airfoil at $\alpha_0 = -0.5$ deg

Fig. 3 Steady pressure distributions for Mach numbers from $M = 0.75$–0.80.

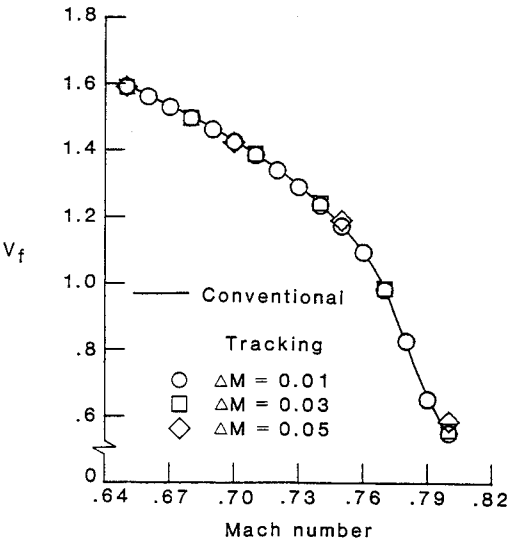

a) NACA 64A010A airfoil at $\alpha_0 = 1.0$ deg

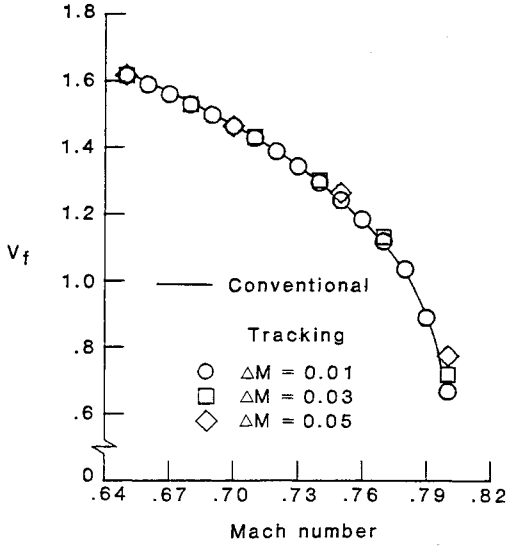

b) MBB-A3 airfoil at $\alpha_0 = -0.5$ deg

Fig. 4 Comparison of flutter boundaries calculated with conventional and flutter boundary tracking procedures.

Transonic flutter boundaries for the NACA 64A010A and MBB-A3 airfoils are shown in Figs. 4a and 4b, respectively. Flutter boundary tracking results are presented for steps in Mach number of $\Delta M = 0.01$, 0.03, and 0.05. The three sets of results were obtained to assess the accuracy and robustness of the tracking procedure by making direct comparisons with conventional solutions. For the two airfoils, the flutter boundaries are quite similar. As pointed out in Ref. 16, the boundary for the MBB-A3 airfoil is nearly identical to that of the NACA 64A010A airfoil when it is shifted to the left by 0.01 Mach number. These flutter boundaries show the so-called transonic dip, but for the Mach number range considered, the boundaries do not define the minimum flutter speed. The Mach number range is restricted since potential codes are not reliable beyond about $M = 0.80$ for these airfoils unless the entropy generated by the shock waves is accounted for.[17] For the NACA 64A010A airfoil (Fig. 4a), all three sets of tracking results are in very good agreement with the conventional solution. The average errors for $\Delta M = 0.01$, 0.03, and 0.05 are 0.39, 0.74, and 2.21%, respectively. The damping and speed index values that were used to determine the $\Delta M = 0.03$ tracking results are listed in Table 1. The conventional method flutter speed indicies are labeled $V_{f\text{exact}}$ in Table 1. The tabulated speed indicies indicate that the tracking procedure stays close to the boundary when marching from one Mach number to the next. For the MBB-A3 airfoil (Fig. 4b), the three sets of tracking results are in very good agreement with the conventional solution except at $M = 0.80$. Here, the flutter points for $\Delta M = 0.03$ and 0.05 are slightly overpredicted because of the steepness of the boundary. The average errors for $\Delta M = 0.01$, 0.03, and 0.05 are 0.46, 1.65, and 4.34%, respectively. For the latter two cases, the average error is dominated by the overprediction of the flutter points at $M = 0.80$. An option exists within the current implementation of the flutter boundary tracking procedure to perform an additional response calculation per Mach number to improve accuracy. When this option was exercised for the MBB-A3 airfoil, the average errors for $\Delta M = 0.03$ and 0.05 were significantly reduced to 0.62 and 0.89, respectively. The results presented demonstrate that the flutter boundary tracking procedure is accurate and robust. The tracking

Table 1 Flutter boundary tracking results for the NACA 64A010A airfoil with $\Delta M = 0.03$

M_i	V_1	V_2	$\zeta(V_1) \times 10^2$	$\zeta(V_2) \times 10^2$	M_{i+1}	V_3	V_4	$\zeta(V_3) \times 10^2$	$\zeta(V_4) \times 10^2$	$V_{f_{i+1}}$	$V_{f_{exact}}$
					0.65	1.64	1.58	−0.60	0.21	1.59	1.59
0.65	1.64	1.58	−0.60	0.21	0.68	1.64	1.49	−1.84	0.10	1.50	1.50
0.68	1.64	1.49	−1.84	0.10	0.71	1.49	1.40	−1.24	−0.15	1.39	1.38
0.71	1.49	1.40	−1.24	−0.15	0.74	1.40	1.25	−1.93	−0.12	1.24	1.23
0.74	1.40	1.25	−1.93	−0.12	0.77	1.25	1.02	−3.03	−0.36	0.99	0.97
0.77	1.25	1.02	−3.03	−0.36	0.80	1.02	0.52	−5.06	0.54	0.55	0.55

results were obtained with fewer response calculations than the conventional method results. A computational savings of approximately a factor of two was attained. In all of the remaining results to be presented, the step in Mach number was set equal to 0.02 and only two response calculations per Mach number were performed.

Flutter Boundary Tracking Results Including Static Twist

Flutter boundary calculations including static aeroelastic twist were performed for the NACA 64A010A and MBB-A3 airfoils. The flutter boundaries were calculated for Mach numbers of $M = 0.70$–0.80. The wing root angles of attack were selected as $\alpha_r = 1.0$ deg for the NACA 64A010A airfoil and $\alpha_r = -0.5$ deg for the MBB-A3 airfoil. These root angles of attack are identical to the mean angles of attack α_0 used in the previous section to allow for direct comparison of results with and without static twist. Steady pressure distributions for these airfoils at $M = 0.80$ are shown in Fig. 5. The speed indices used for the steady pressure distributions computed with static twist were the resulting flutter speed values, $V_f = 0.67$ and 0.94, for the NACA 64A010A and MBB-A3 airfoils, respectively. For this case, the static twist decreases the strength of the upper surface shocks and reduces the steady-state loading. For the NACA 64A010A airfoil (Fig. 5a), the static twist lowers the mean angle of attack from $\alpha_0 = 1.0$ to 0.46 deg. This change in mean angle of attack weakens the shock and displaces it forward from 68 to 61% chord. Additionally, a relatively weak shock forms on the lower surface at 49% chord. For the MBB-A3 airfoil (Fig. 5b), the static twist lowers the mean angle of attack from $\alpha_0 = -0.5$ to -1.5 deg. The affect of static twist on the pressure distributions of the MBB-A3 airfoil is similar to that on the NACA 64A010A airfoil. The upper-surface shock wave is significantly weakened and is displaced forward from 68 to 61% chord, which is the same shift in shock location that was determined for the NACA 64A010A airfoil. In general, static twist affected the steady pressure distributions of the two airfoils in a similar manner over the range of Mach numbers considered. The static twist angles for both airfoils are plotted as functions of Mach number in Fig. 6. These angles were computed at the speed indices corresponding to flutter (to be presented subsequently). Only results from the flutter boundary tracking procedure are plotted since the conventional method twist angles are identical to plotting accuracy. As shown in Fig. 6, the twist angles decrease with increasing Mach number since the flutter speed index decreases. The static twist for the MBB-A3 airfoil is much larger (negatively) than that of the NACA 64A010A airfoil throughout the entire Mach number range considered. This is attributed to the different pitching moment characteristics of the MBB-A3 airfoil due to the aft loading.

Flutter boundary tracking results, computed both with and without static twist, are shown in Figs. 7a and 7b for the NACA 64A010A and MBB-A3 airfoils, respectively. These results are compared with conventional method solutions to assess the accuracy of the tracking procedure when static twist is included. The results computed without static twist are those shown previously in Figs. 4a and 4b. The overall effect of static twist on the flutter behavior of both airfoils is

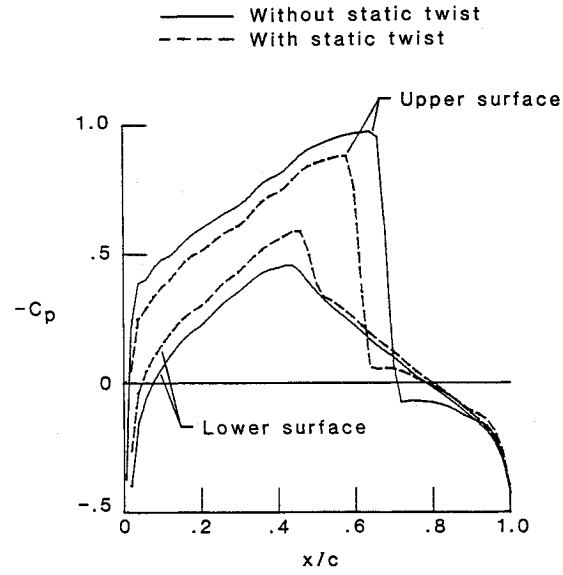

a) NACA 64A010A airfoil with $\alpha_r = 1.0$ deg

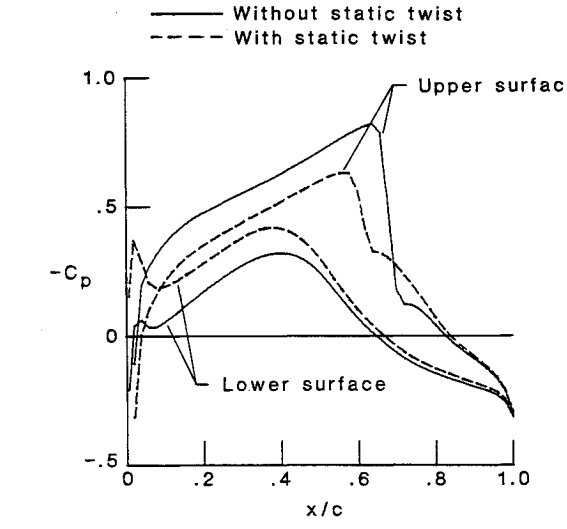

b) MBB-A3 airfoil with $\alpha_r = -0.5$ deg

Fig. 5 Steady pressure distributions at $M = 0.80$, including the effect of static aeroelastic twist at flutter.

an increase in flutter speed index. Static aeroelastic effects on flutter speed index vary as the twist angles change with speed index and Mach number. For example, at subcritical Mach numbers, static twist has little affect on flutter behavior, as would be expected based upon linear theory. As the Mach number increases into the transonic regime, the effects of static twist on flutter generally increase. For the NACA 64A010A airfoil (Fig. 7a), the flutter boundaries with and without static twist show only small differences between

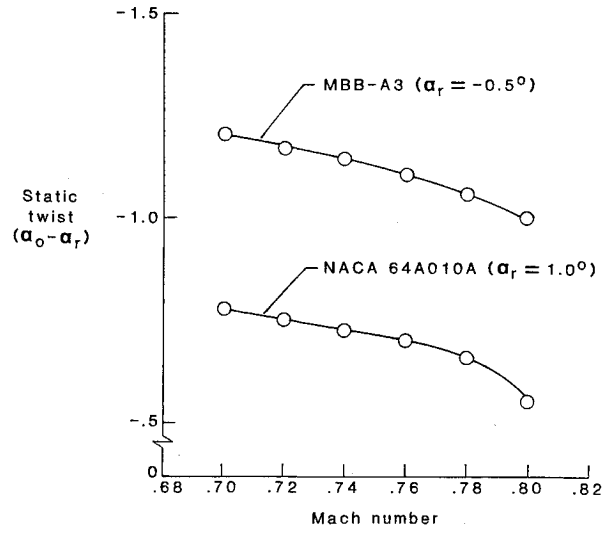

Fig. 6 Static aeroelastic twist angle ($\alpha_0 - \alpha_r$) for the NACA 64A010A and MBB-A3 airfoils at flutter.

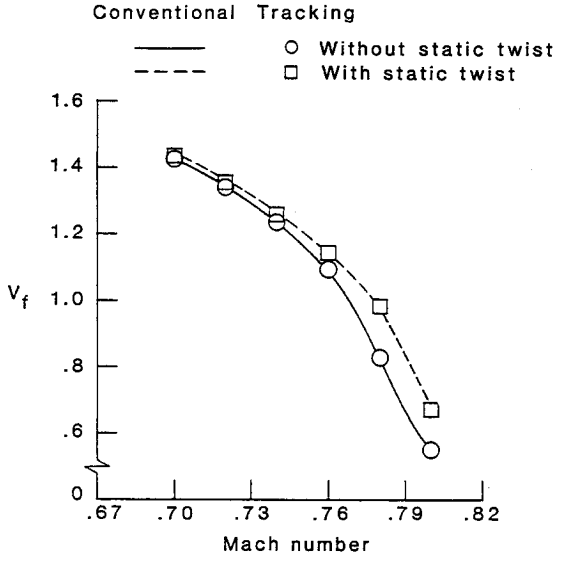

a) NACA 64A010A airfoil with $\alpha_r = 1.0$ deg

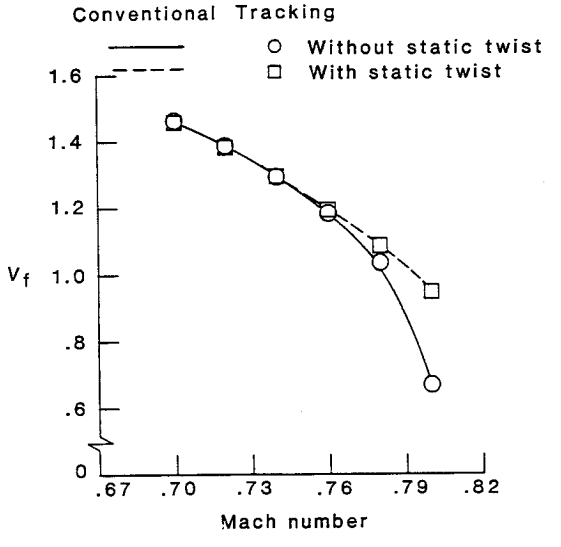

b) MBB-A3 airfoil with $\alpha_r = -0.5$ deg

Fig. 7 Comparison of flutter boundaries calculated with conventional and flutter boundary tracking procedures including static aeroelastic twist.

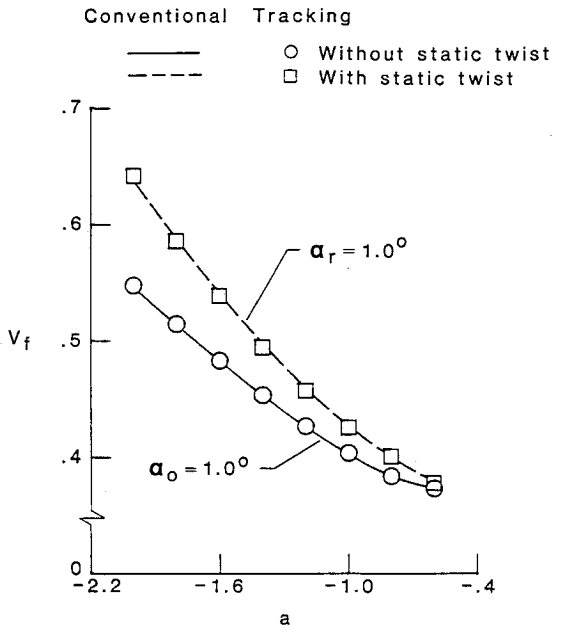

Fig. 8 Flutter boundaries as a function of elastic axis location for the NACA 64A010A airfoil at $M = 0.80$.

$M = 0.70$ and 0.74. At $M = 0.76$, the flow is slightly supercritical and the static twist begins to have a larger effect on flutter. A shock forms on the airfoil upper surface between $M = 0.76$ and 0.78, which produces a large increase in flutter speed index due to static twist. At $M = 0.78$–0.80, the static twist angle decreases and its effect on the flutter boundary is slightly reduced. For the MBB-A3 airfoil (Fig. 7b), there is a negligible difference in the flutter boundaries with and without static twist below $M = 0.76$, due to the subcritical nature of the flow. Between $M = 0.76$ and 0.78, the shock wave forms and static twist begins to affect the flutter boundary for the MBB-A3 airfoil in a manner similar to that for the NACA 64A010A airfoil. At $M = 0.80$, however, a more significant increase in the flutter speed index occurs for the MBB-A3 airfoil due to the much larger (negative) static twist angle, as shown in Fig. 6. A much larger value for flutter speed index also results, since the shock wave on the MBB-A3 airfoil is much weaker in comparison with the NACA 64A010A airfoil. Edwards et al.[7] studied the effects of static twist for higher root angles of attack ($\alpha_r = 2$–5 deg) where they found more pronounced differences in the flutter boundaries of the two airfoils. The tracking procedure flutter boundaries including static twist in Fig. 7 are in excellent agreement with the respective conventional method solutions. The average errors for the boundaries with static twist are 0.32 and 0.19% for the NACA 64A010A and MBB-A3 airfoils, respectively. The differences in the flutter boundary results with and without static twist demonstrate the importance of static deformation on flutter behavior. The inclusion of static twist is therefore a requirement for performing realistic flutter analyses for wings. The tracking procedure thus contains all of the essential features for application to practical three-dimensional cases.

Flutter Boundary Tracking Results as a Function of Elastic Axis Location

Flutter boundary tracking results as a function of elastic axis location are shown in Fig. 8 for the NACA 64A010A airfoil at $M = 0.80$. Calculations were performed both with and without static aeroelastic twist. The airfoil mass properties were held fixed by requiring that $x_\alpha = -(a + 0.2)$, which fixes the mass center, and that $r_\alpha^2 = r_{cg}^2 + x_\alpha^2$ (where $r_{cg} = 0.49$), which fixes the radius of gyration about the center of gravity r_{cg}. The step in elastic axis location was

selected as $\Delta a = 0.2$ and flutter boundaries were calculated for the range $-2.0 \le a \le -0.6$. The results for $a = -2.0$ are the same as those shown in Fig. 7a at $M = 0.80$. As shown in Fig. 8, the flutter speed index decreases as the elastic axis location is moved aft from $a = -2.0$ to -0.6. The decrease in speed index is due to a lower pitch mode frequency, which increases the coupling between the plunge and pitch modes. For example, at $a = -2.0$, the wind-off coupled plunge and pitch natural frequencies are 71.33 and 535.65 rad/s, respectively. At $a = -0.6$, these frequencies become 78.23 and 165.26 rad/s, respectively. The flutter boundary with static twist has flutter speed indices that are greater than those for the boundary without static twist. This increase in flutter speed index due to static twist is a function of the twist angle $(\alpha_0 - \alpha_r)$. The twist angles decrease from $(\alpha_0 - \alpha_r) = -0.54$ deg at $a = -2.0$ to $(\alpha_0 - \alpha_r) = -0.36$ deg at $a = -0.6$. Consequently, the increase in flutter speed index due to static twist is greatest at $a = -2.0$.

Conclusions

An automated flutter boundary tracking procedure has been developed for the efficient calculation of transonic flutter boundaries. This new procedure uses aeroelastic responses computed with the XTRAN2L unsteady transonic small-disturbance code to march along the boundary by taking steps in speed and Mach number. The flutter boundary tracking procedure therefore reduces the number of response calculations previously required to determine a transonic flutter boundary and provides a complete boundary in a single job submission. Furthermore, the tracking procedure reduces computational costs, since only two response calculations are required per Mach number.

Flutter boundary results were presented for a simple aeroelastic system consisting of a typical airfoil section oscillating with pitch and plunge degrees of freedom to demonstrate the tracking procedure. These flutter boundaries were in good agreement with "exact" boundaries calculated using the conventional method. With the flutter boundary tracking procedure, the elapsed analysis time has been reduced from 2-4 weeks to 1 day turnaround and the computational cost approximately halved.

To be able to conceptually apply the tracking procedure to realistic three-dimensional cases, the procedure was extended to include static aeroelastic twist as a two-dimensional simulation of the static deformation of a wing. The tracking procedure flutter boundaries computed with static twist were in excellent agreement with the "exact" solution and cost no more than the boundaries obtained without static twist. Therefore, the flutter boundary tracking procedure is accurate and contains all of the essential features that are required to apply it to practical three-dimensional cases.

Additionally, the tracking procedure is not constrained to determine flutter boundaries as a function of Mach number. The procedure is applicable to other parameters influencing the flutter boundary, making it potentially useful as a design tool. A sample calculation was presented showing a flutter boundary as a function of elastic axis location, thereby demonstrating this capability.

Acknowledgment

This work constitutes a part of the first author's M.S. thesis at Purdue University and was supported by the NASA Langley Graduate Aeronautics Program under Grant NAG-1-372.

References

[1]Ballhaus, W.F. and Goorjian, P.M., "Computation of Unsteady Transonic Flows by the Indicial Method," *AIAA Journal,* Vol. 16, Feb. 1978, pp. 117-124.

[2]Ballhaus, W.F. and Goorjian, P.M., "Implicit Finite-Difference Computations of Unsteady Transonic Flows About Airfoils," *AIAA Journal,* Vol. 15, Dec. 1977, pp. 1728-1735.

[3]Guruswamy, P. and Yang, T.Y., "Aeroelastic Time Response Analysis of Thin Airfoils by Transonic Code LTRAN2," *Journal of Computers and Fluids,* Vol. 9, Dec. 1981, pp. 409-425; also, AFFDL-TR-79-3077, June 1979.

[4]Rizzetta, D.P., "Time-Dependent Responses of a Two-Dimensional Airfoil in Transonic Flow," *AIAA Journal,* Vol. 17, Jan. 1979, pp. 26-32.

[5]Yang, T.Y. and Chen, C. H., "Transonic Flutter and Response Analyses of Two Three-Degree-of-Freedom Airfoils," *Journal of Aircraft,* Vol. 19, Oct. 1982, pp. 875-774; also, AFWAL-TR-81-3102, Aug. 1981.

[6]Yang, T.Y. and Batina, J.T., "Transonic Time-Response Analysis of Three D.O.F. Conventional and Supercritical Airfoils," *Journal of Aircraft,* Vol. 20, Aug. 1983, pp. 703-710.

[7]Edwards, J.W., Bennett, R.M., Whitlow, W. Jr., and Seidel, D.A., "Time-Marching Transonic Flutter Solutions Including Angle-of-Attack Effects," *Journal of Aircraft,* Vol. 20, Nov. 1983, pp. 899-906.

[8]Batina, J.T. and Yang, T.Y., "Transonic Time Responses of the MBB A-3 Supercritical Airfoil Including Active Controls," *Journal of Aircraft,* Vol. 22, May 1985, pp. 393-400.

[9]Berry, H.M., Batina, J.T., and Yang, T.Y., "Viscous Effects on Transonic Airfoil Stability and Response," AIAA Paper 85-0586, April 1985.

[10]Borland, C.J. and Rizzetta, D.P., "Nonlinear Transonic Flutter Analysis," *AIAA Journal,* Vol. 20, Nov. 1982, pp. 1606-1615.

[11]Whitlow, W. Jr., "XTRAN2L: A Program for Solving the General-Frequency Unsteady Transonic Small Disturbance Equation," NASA TM-85723, Nov. 1983.

[12]Bennett, R.M. and Desmarais, R.N., "Curve Fitting of Aeroelastic Transient Response Data with Exponential Functions in Flutter Testing Techniques," NASA SP-415, 1975, pp. 43-58.

[13]Bland, S.R., "AGARD Two-Dimensional Aeroelastic Configurations," AGARD-AR-156, Aug. 1979.

[14]Isogai, K., "Numerical Study of Transonic Flutter of a Two-Dimensional Airfoil," National Aerospace Laboratory, Japan, Rept. TR-617T, July 1980.

[15]Isogai, K., "On the Transonic Dip Mechanism of Flutter of a Sweptback Wing," *AIAA Journal,* Vol. 17, July 1979, pp. 793-795.

[16]Bland, S.R. and Edwards, J.W., "Airfoil Shape and Thickness Effects on Transonic Airloads and Flutter," *Journal of Aircraft,* Vol. 21, March 1984, pp. 209-217.

[17]Fuglsang, D.F. and Williams, M.H., "Non-Isentropic Unsteady Transonic Small Disturbance Theory," AIAA Paper 85-0600, April 1985.